AIAA/AAS Astrodynamics Specialist Conference
18-21 August 2008, Honolulu, Hawaii

AIAA 2008-6438

A New Empirical Thermospheric Density Model JB2008 Using New Solar and Geomagnetic Indices

Bruce R. Bowman*
Air Force Space Command
Space Analysis / A9AC
bruce.bowman@peterson.af.mil
719-556-3710

W. Kent Tobiska
Space Environment Technologies
ktobiska@spacenvironment.net
310-573-4185

Frank A. Marcos, Cheryl Y. Huang, Chin S. Lin, William J. Burke
Air Force Research Laboratory
AFRL /RVBXT
AFRL.RVB.PA@hanscom.af.mil
781-377-3037

A new empirical atmospheric density model, Jacchia-Bowman 2008, is developed as an improved revision to the Jacchia-Bowman 2006 model which is based on Jacchia's diffusion equations. Driving solar indices are computed from on-orbit sensor data are used for the solar irradiances in the extreme through far ultraviolet, including x-ray and Lyman-α wavelengths. New exospheric temperature equations are developed to represent the thermospheric EUV and FUV heating. New semiannual density equations based on multiple 81-day average solar indices are used to represent the variations in the semiannual density cycle that result from EUV heating. Geomagnetic storm effects are modeled using the Dst index as the driver of global density changes. The model is validated through comparisons with accurate daily density drag data previously computed for numerous satellites in the altitude range of 175 to 1000 km. Model comparisons are computed for the JB2008, JB2006, Jacchia 1970, and NRLMSIS 2000 models. Accelerometer measurements from the CHAMP and GRACE satellites are also used to validate the new geomagnetic storm equations.

I. Introduction

Until development of the Jacchia-Bowman 2006 (JB2006) model[1] typical density model errors on the order of 15%-20% one standard deviation were recognized for all empirical models[2] developed since the mid 1960s. These large density standard deviations correspond to maximum density errors of approximately 40-60% as observed in satellite drag data. There are two main reasons for these consistently large values. One is the result of not modeling the semiannual density variation[3,4] as a function of solar activity, and the other results from not modeling the full thermospheric heating from solar ultraviolet radiation. Geomagnetic storms provide episodic, and overall smaller, contributions to the standard deviation. All models prior to JB2006 have used the F_{10} and 81-day centered average $\overline{F}_{10}$ proxies as representative of the solar ultraviolet (UV) heating. However, the unmodeled errors derived from satellite drag data all show very large density errors with approximately 27-day periods, representing one solar rotation cycle. These errors are the result of not fully modeling the ultraviolet radiation effects on the thermosphere, which have a one solar rotation periodicity. The purpose of this paper is to describe the further development of the Jacchia-Bowman models that incorporate new solar indices, a new semiannual density model, and a new geomagnetic index model.

II. Density Data Sources

Four different density data sources were used in the development of the JB2008 model. These sources included Air Force daily density values from 1997 through 2007, Air Force HASDM densities values from 2001 through 2005, CHAMP accelerometer densities from 2001 through 2005, and GRACE accelerometer densities from 2002 through 2005.

The daily density values consist of very accurate daily values[5] obtained from drag analysis of numerous satellites with perigee altitudes of 175 km to 1000 km. Daily temperature corrections to the Air Force modified Jacchia 1970 atmospheric model[6,7] were obtained from the satellite data throughout the period 1997 through 2007. Approximately 210,000 daily temperature values were computed using a special energy dissipation rate (EDR) method[5], where radar and optical observations are fit with special orbit perturbations. For each satellite tracked approximately 100,000 radar and optical observations were available for the special perturbation orbit fitting. A differential orbit correction program was used to fit the observations to obtain the standard 6 Keplerian elements plus the ballistic coefficient. "True" ballistic coefficients[8] were then used with the observed daily temperature corrections to obtain daily density values. The daily density computation was validated by comparing historical daily density values computed for the last 30 years for over 30 satellites. The accuracy of the density values was determined from comparisons of geographically overlapping perigee location data, with over 8500 pairs of density values used in the comparisons. The density errors were found to be less than 4% overall, with errors on the order of 2% for values covering the latest solar maximum.

Density values were also obtained from the HASDM[9,10] model. The Air Force Space Command's High Accuracy Satellite Drag Model (HASDM) processes drag information from the trajectories of 75 to 80 inactive payloads and debris (*calibration satellites*) to solve for a dynamically changing global correction to the thermosphere. This correction covers the altitude range of ~200 to 800 km. Satellite tracking observations (azimuth, elevation, range, and range rate) from the Air Force Space Surveillance Network (SSN) are processed directly to derive the neutral atmospheric density. Thermospheric density correction parameters are computed along with the trajectory states of the calibration satellites in a single estimation process, known as the Dynamic Calibration Atmosphere (DCA). This is a weighted least squares differential correction across all calibration satellites that simultaneously solve for global density corrections and a state vector for each calibration satellite. DCA uses the Jacchia 1970 thermosphere as its base model. DCA estimates 13 global temperature correction parameters every 3 hours, while the state vector of each calibration satellite is estimated for a 2-day fit span. The 13 global temperature correction parameters produce a spatial resolution of approximately 80 degree geographical blocks. The HASDM and DCA programs have been previously well documented[9,10]. For the JB2008 model development densities were computed every 10 seconds along the CHAMP and GRACE orbits using the HASDM temperature coefficients obtained for the 2001 through 2005 time period.

Another density data source came from the CHAMP (CHAllenging Minisatellite Payload) satellite, a German small satellite mission for geoscientific and atmospheric research and applications, managed by GFZ[11], Potsdam. CHAMP was launched on July 15, 2000 into an almost circular, near-polar orbit (inclination 87.2°) with an initial average altitude of 450 km. CHAMP carries a very sensitive STAR accelerometer, the data of which can be used to derive neutral densities[12]. Densities every 10 seconds were available for the 2001 through 2005 time period.

A fourth density data source used in this model development came from the GRACE satellite mission (Gravity Recovery and Climate Experiment)[13], the mission objective being to map the global gravity field with unprecedented accuracy. GRACE is a twin satellite configuration, which was launched on March 17, 2002 into an almost circular, near-polar orbit (inclination 89.0°) with an initial altitude of 500 km. GRACE carries extremely sensitive SuperSTAR accelerometers which are an order of magnitude more precise than STAR. Densities every 5 seconds were available[14] for the 2002 through 2005 time period.

III. Global Nighttime Minimum Exospheric Temperature

A. Temperature Description

The variations in the ultraviolet solar radiation that heats the earth's thermosphere consists of two components, one related to solar rotational modulation of active region emission, and the other long-term evolution of the main solar magnetic field[6,7]. The passage of active regions across the disk during a solar rotation period produces irradiance variations of approximately 27 days, while the main solar magnetic field evolution produces irradiance variations over approximately 11 years. The 10.7-cm solar flux, F_{10}, has in the past been used to represent these effects. However, new solar indices have been recently[15] used to compute better density variation correlations with ultraviolet radiation covering the entire Far UV as well as the EUV wavelengths.

In determining a new global nighttime minimum exospheric temperature Tc equation with the new solar indices, the density values were converted into daily Tc temperature values using the Jacchia 70 empirical atmospheric density model. To obtain accurate Tc values the large semiannual density variations had to be correctly modeled. A major density variation, aside from the 11-year and 27-day solar heating effect, is the semiannual change. This can be as large as 250% from a July minimum to an October maximum during solar maximum years, and as small as 60% from July to October during solar minimum years (at 600 km)[3]. The semiannual variation was computed on a yearly basis from the previously derived density data. Jacchia's 70 semiannual density model equation was then replaced using these observed semiannual yearly variations. A smaller correction to Jacchia's model was also made for the observed errors in the latitude and local solar time density variations. From these different model corrections an accurate Tc value, due almost entirely to solar heating, was obtained.

The solar UV absorption spectrum in the thermosphere was analyzed to determine the new solar indices required for the new temperature equation development. The solar index F_{10} is really a proxy index because it is measured at a 10.7-cm wavelength, which is not a direct measure of any ultraviolet radiation and is not absorbed by the atmosphere. Direct ultraviolet heating indices were recently developed that represent the extreme (EUV), far (FUV), and mid (MUV) solar UV radiation. Previous analyses[15] suggested that EUV and FUV indices[26] were required to capture most of the thermospheric heating, and an additional improvement could be obtained by using an index representing UV energy absorption at lower thermospheric altitudes than by using previous EUV and FUV indices. The daily indices selected for this model development include F_{10}, S_{10}, M_{10}, and Y_{10}.

F_{10}: The 10.7-cm solar radio flux, F_{10}, is produced daily by the Canadian National Research Council's Herzberg Institute of Astrophysics at its ground-based Dominion Radio Astrophysical Observatory located in Penticton, British Columbia. The physical units of F_{10} are W m^{-2} Hz^{-1} and more conveniently expressed in solar flux units (1 sfu = 1×10^{-22} W m^{-2} Hz^{-1}). A running 81-day centered smoothed set of values using the moving boxcar method was created, and these data are referred to as $\overline{F}_{10}$. Linear regression with daily F_{10} has been used to scale and report all other solar indices in units of sfu.

S_{10}: The NASA/ESA Solar and Heliospheric Observatory (SOHO) research satellite uses the Solar Extreme-ultraviolet Monitor (SEM) instrument that has been measuring the 26–34 nm solar EUV emission since launch in December 1995. This integrated 26–34 nm emission, which is also measured by the post-GOES 12 operational satellites, has been normalized and converted to sfu through linear regression with F_{10}, producing the new index S_{10}. The broadband (wavelength integrated) SEM 26-34 nm irradiances are EUV line emissions dominated by the chromospheric He II line at 30.4 nm with contributions from other chromospheric and coronal lines. This energy principally comes from solar active regions. A running 81-day centered smoothed set of values using the moving boxcar method was created, and these data are referred to as $\overline{S}_{10}$.

M_{10}: The NOAA series of operational satellites host the Solar Backscatter Ultraviolet (SBUV) spectrometer that has the objective of monitoring ozone in the Earth's lower atmosphere. In its discrete operating mode, a diffuser screen is placed in front of the instrument's aperture in order to scatter solar MUV radiation near 280 nm into the instrument. This solar spectral region contains both photospheric continuum and chromospheric line emissions. The chromospheric Mg II *h* and *k* lines at 279.56 and 280.27 nm, respectively, and the weakly varying photospheric wings (or continuum longward and shortward of the core line emission), are operationally observed by the instrument. The Mg II core-to-wing ratio (cwr) is calculated between the variable lines and nearly non-varying wings. The result is a measure of chromospheric and some photospheric solar active region activity independent of instrument sensitivity change through time, and is referred to as the Mg II cwr. The Mg II cwr have been used in a linear regression with F_{10} to derive the M_{10} index in sfu units. A running 81-day centered smoothed set of values using the moving boxcar method was created, and these data are referred to as $\overline{M}_{10}$.

Y_{10}: The operational GOES X-ray Spectrometer (XRS) instrument provides the 0.1–0.8 nm solar X-ray emission. X-rays in the 0.1–0.8 nm range come from the cool and hot corona and are typically a combination of both very bright solar active region background that varies slowly (days to months) plus flares that vary rapidly (minutes to hours), respectively. The photons arriving at Earth are primarily absorbed in the mesosphere and lower thermosphere (80–90 km) by molecular oxygen and nitrogen where they ionize those neutral constituents to create the ionospheric D-region. An index of the solar X-ray active region background, without the flare component, has been developed. This is called the X_{10} index[27]. The 0.1-0.8 nm X-rays are a major energy source in these atmospheric regions during high solar activity but relinquish their dominance to the competing hydrogen (H) Lyman-α emission during moderate and low solar activity. Lyman-α is also deposited in the same atmospheric regions, is created in the solar upper chromosphere and transition region, and demarcates the EUV from the FUV spectral regions[28]. It is formed primarily in solar active regions, plage, and network; the photons, arriving at Earth, are absorbed in the mesosphere and lower thermosphere where they dissociate nitric oxide (NO) and participate in water (H_2O) chemistry. Lyman-α has been observed by the SOLSTICE instrument on the UARS and SORCE NASA research satellites as well as by the SEE instrument on NASA TIMED research satellite. Since these two solar emissions are competing drivers to the mesosphere and lower thermosphere, we have developed a mixed solar index Y_{10}. It is weighted to represent mostly X_{10} during solar maximum and to represent mostly Lyman-α during moderate and low solar activity. The independent, normalized $\overline{F}_{10}$ is used as the weighting function and multiplied with the X_{10} and Lyman-α as fractions to their solar maximum values.

B. Tc Temperature Equation

Previous analyses[16,17] of different density model errors have shown that using the $\overline{F}_{10}$ index to capture the 11-year solar cycle variation does not fully represent the entire thermospheric heating, especially during solar minimum conditions. It has been shown that real density-to-model ratios have drops of 30-40% at solar minimum. The $\overline{F}_{10}$ index has long been known to "flatten-out" around solar minimum, while the real EUV heating continues to show variability. However, a previous analysis[15] demonstrated that the $\overline{F}_{10}$ index was still better at representing the full 11-year cycle changes than either the $\overline{S}_{10}$ or $\overline{M}_{10}$ index. Therefore, it was decided to use the $\overline{F}_{10}$ index for the great majority of the time, but supplementing it with the EUV $\overline{S}_{10}$

during solar minimum times. With this approach a new 11-year solar index was developed with the following weighting scheme:

$$\overline{F}_S = \overline{F}_{10} \text{ x } W_T + \overline{S}_{10} \text{ x } (1\text{-}W_T) \quad \text{where} \quad W_T = \sqrt[4]{\left(\overline{F}_{10} / 240\right)} \tag{1}$$

With this new index the solution of the best nighttime minimum exospheric Tc equation was obtained using numerous satellites for the years from 1997 through 2007 when all new solar indices were available. The resulting equation is:

$$Tc = 392.4 + 3.227\,\overline{F}_S + 0.298\,\Delta F_{10} + 2.259\,\Delta S_{10} + 0.312\,\Delta M_{10} + 0.178\,\Delta Y_{10} \tag{2}$$

The delta values (ΔF_{10}, ΔS_{10}, ΔM_{10}, ΔY_{10}) represent the difference of the daily and 81-day centered average value of each index. The 81-day (3-solar rotation period) centered value was previously[15] determined to be the best long term average to use. In the solution the 2007 solar minimum data was heavily weighted to help better define the density variations during solar minimum times. To avoid increases in Tc due to geomagnetic storms all daily data with the geomagnetic index $a_p >= 30$ were rejected. This meant that if a solar index required a lag time of 5 days, each of the 5 days prior to the current time had to have $a_p < 30$ for the current daily density data to be used.

It was determined that a lag time of 1 day was the best to use for the F_{10} and S_{10} indices. For using the M_{10} index an analysis determined that the best (least squares minimum) lag time was 2 days, and for Y_{10} a best lag time of 5 days was obtained.

Initially for the JB2006 model, which did not use Y_{10}, the lag time for M_{10} was determined to be 5 days. The M_{10} index was previously accounting for the longer lag times in the lower thermosphere. However, with the addition of the low altitude Y_{10} index the M_{10} lag time became shorter, and the low altitude longer absorption lag time was captured by Y_{10} combining absorption of X-Rays and Lyman-α at altitudes around 80-90 km.

In-order to evaluate the new Tc equation the "observed" density-to-model ratios were computed for both the JB2006 and new JB2008 models, the Jacchia 70 model, and the NRLMSIS[18] model. The new JB2008 semiannual equations, discussed in the following sections, were used in the JB2008 evaluation. The "observed" densities were obtained by using the computed 3-hour spherical harmonic HASDM temperature correction coefficients, and computing density values at 10 minute steps along the CHAMP reference orbits obtained for 2001 through 2007. These HASDM-to-Model ratios were then binned by $\overline{F}_{10}$ and plotted in Figure 1. It can be readily seen that all the previous models using just $\overline{F}_{10}$ for the 11-year cycle variations show a significant decrease in the ratios at solar minimum conditions. The JB2008 model does much better at representing the solar minimum density decrease, although it still does not completely capture the density variation. Figure 2 shows the density model standard deviations binned again by $\overline{F}_{10}$. The much larger sigma at solar minimum (very low $\overline{F}_{10}$) are a direct result of the model ratio errors at low $\overline{F}_{10}$. The new JB2008 Tc equation is a significant improvement over all other models in representing the solar thermospheric heating.

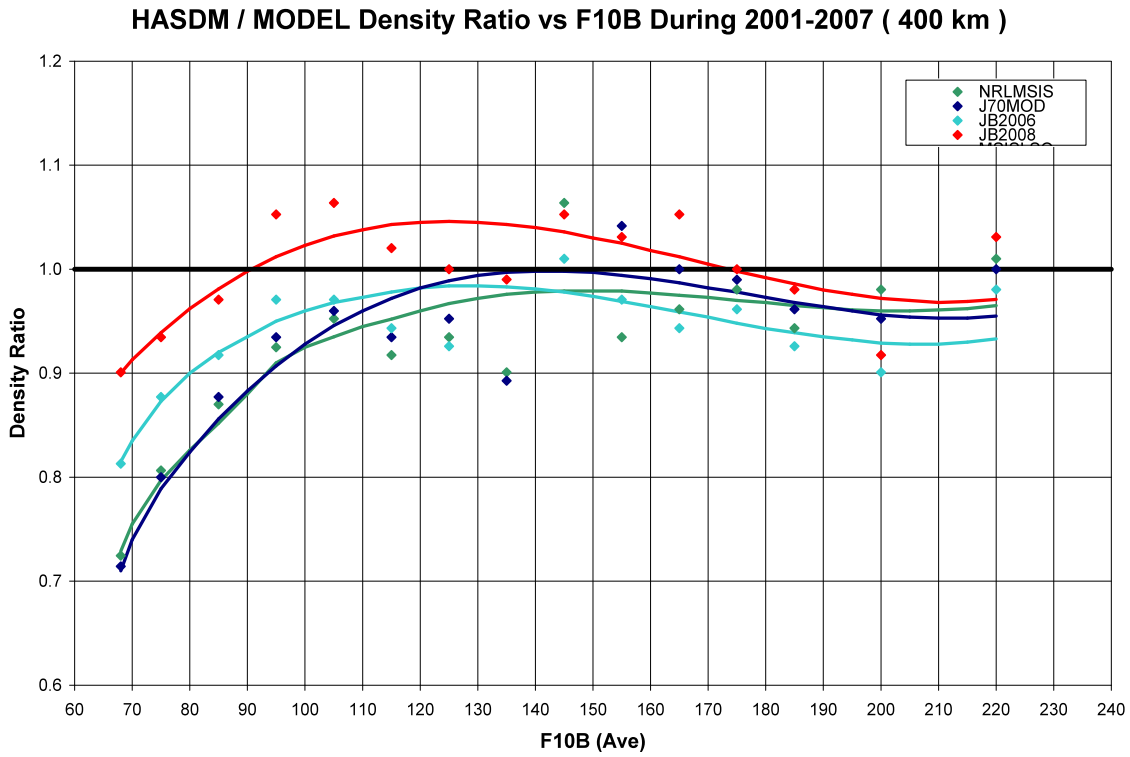

Figure 1. HASDM-to-Model density ratios at 400km altitude as a function of $\overline{F}_{10}$ (F10B).

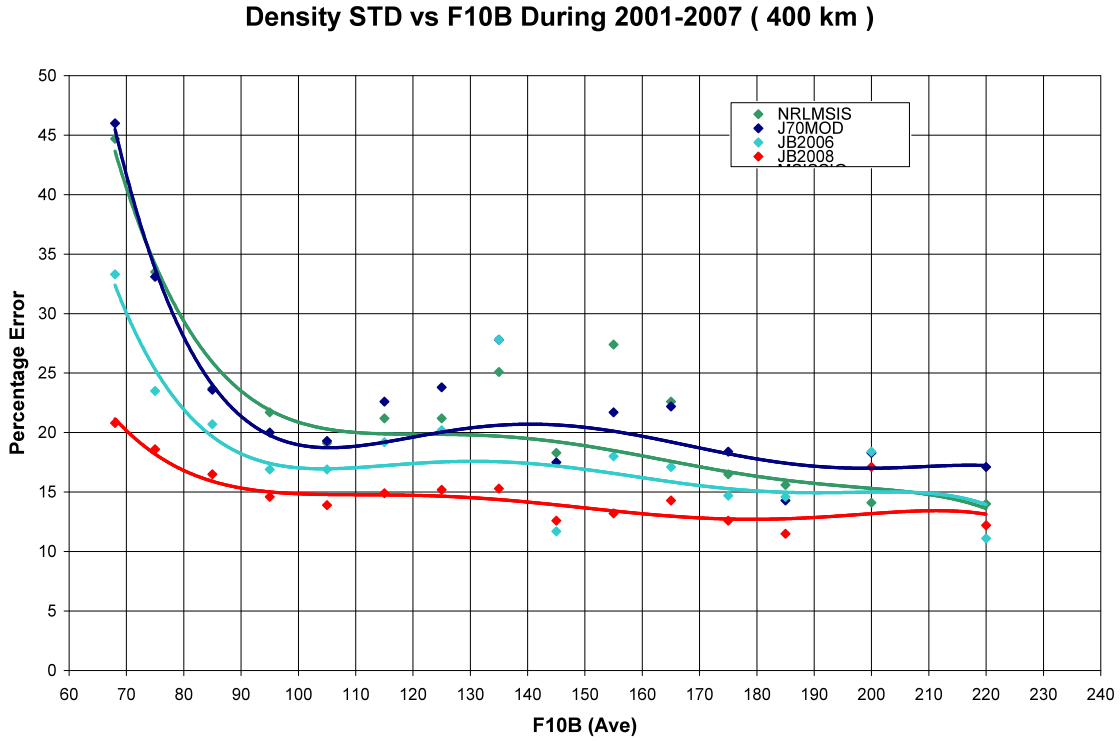

Figure 2. Density percentage errors (1 standard deviation) from model density values at 400 km altitude compared to HASDM density values.

IV. Semiannual Density Variation

The semiannual density variation was first discovered in 1961[19]. Paetzold and Zschorner observed a global density variation from analysis of satellite drag data, which showed a 6-month periodicity maximum occurring in April and October, and minimum occurring in January and July. Many authors, such as King-Hele[20] and Jacchia[6,7], analyzed the semiannual effect from satellite drag during the 1960s and early 1970s. They found that the semiannual variation was a worldwide effect with the times of the yearly maximum and minimum occurring independent of height. However, the semiannual period was found to be only approximate, as the times of occurrence of the minima and maxima seemed to vary from year to year. Generally the October maximum exceeded that in April and the July minimum was deeper than that in January. The main driving mechanism for the observed variability in the semiannual effect remained a mystery. Jacchia first modeled the effect as a temperature variation which included a function of the 81-day solar flux $\overline{F}_{10}$ index. However, he soon discovered difficulties with the temperature model, and eventually modeled the semiannual variation as a density variation. He also dropped the $\overline{F}_{10}$ dependence, suggesting that he did not have enough data to support this solar flux relationship. He found that the amplitude of the semiannual density variation was strongly height-dependent and variable from year to year. However, he could not show a definitive correlation of the variation with solar activity.

A. Semiannual Density Variation Function

Jacchia obtained the following equations from analysis of 12 years of satellite drag data. He represented the semiannual density variation in the form:

$$\Delta_{SA} \log_{10} \rho = F(z)\, G(t) \tag{3}$$

G(t) represents the average density variation as a function of time in which the amplitude (i.e. the difference in $\log_{10}$ density between the principal minimum in July and the principle maximum in October) is normalized to 1, and F(z) is the relation between the amplitude and the height z.

From previous analysis[3] it was determined that a Fourier series could accurately represent Jacchia's G(t) equation structure. A 9-term coefficient series, including frequencies up to 4 cycles per year, was sufficient to capture all the yearly variability in G(t) that had been previously observed by Jacchia. It was also determined that a simplified quadratic polynomial equation in z could sufficiently capture Jacchia's F(z) equation and not lose any fidelity in the observed F(z) values.

B. Semiannual F(z) Height Function

For the Jacchia-Bowman model developments the amplitude, F(z), of the semiannual variation was determined[3,4] on a year-by-year and satellite-by-satellite basis. The smoothed density difference data was fit each year for each satellite using a 9 term Fourier series. The F(z) value was then computed from each fit as the difference between the minimum and maximum values for the year.

Figure 3 shows the results of three different years of data, along with the plot of Jacchia's F(z) equation. For each year, the F(z) values were fit with a quadratic polynomial in height. The smoothed curves shown in Figure 3 represent the least squares quadratic fit obtained for three different years. The F(z) $\Delta\log_{10}\rho$ data for all satellites are very consistent within each year. The most notable feature in Figure 3 is the very large difference in maximum amplitude among the years displayed. The 2002 data shows a maximum density variation of 250% near 800km, while the 1993 data shows only a 60% maximum variation. Jacchia's F(z) function only gives a constant 130% maximum variation for all years.

Previous development of the JB2006 model showed that solar EUV and FUV heating played an important part in thermospheric density variations. Bowman[4] extended the previous semiannual work[3] to include additional solar EUV indices in an attempt to capture the remaining semiannual variations not modeled by the JB2006 model.

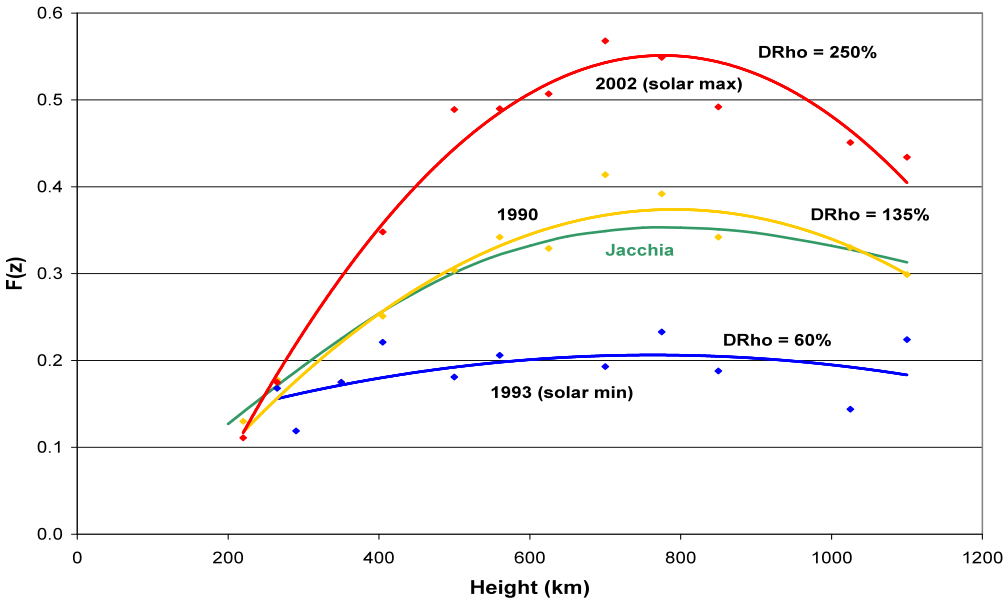

Figure 3. The amplitude function F(z) for three different years (1990, 1993, 2002), with semiannual amplitudes plotted for each satellite for each year. The constant F(z) function from Jacchia is also plotted.

Roble[21] computed the thermospheric temperature response to solar EUV heating using his coupled thermosphere and ionosphere global average model. He found that removing the He II 30.4 nm emission produced the largest (by a factor of 2) temperature change. Therefore, it was very important to select an EUV index that captured the emission of this He II irradiance line. These results together with previous analysis[15] of thermospheric response to new solar indices suggested a new set of solar indices to use for the semiannual variation. New 81-day centered $\overline{S}_{10}$ and $\overline{M}_{10}$ indices were computed for use along with the previous $\overline{F}_{10}$ index. Previous work[4] determined the new solar index for F(z) to be

$$\overline{F}_{SMJ} = 1.00\ \overline{F}_J - 0.70\ \overline{S}_J - 0.04\ \overline{M}_J \tag{4}$$

where the $\overline{F}_J$, $\overline{S}_J$, and $\overline{M}_J$ indices represent the July averages of the $\overline{F}_{10}$, $\overline{S}_{10}$, and $\overline{M}_{10}$ indices respectively. This $\overline{F}_{SMJ}$ index was then used to determine which terms were significant in defining a new F(z) equation. The resultant new F(z) equation, with z = height/1000, using the new index was determined to be

$$F(z) = B_1 + B_2\overline{F}_{SMJ} + B_3 z\overline{F}_{SMJ} + B_4 z^2\overline{F}_{SMJ} + B_5 z\overline{F}^2_{SMJ} \tag{5}$$

Table 1 lists the resulting B coefficient values with their standard deviations obtained from using Equation (4) for the solar index required in Equation (5). The standard deviations of all the coefficients are an order of magnitude less than the coefficient values, indicating that all five coefficients have been well determined.

Equation (5) using $\overline{F}_{SMJ}$ represents a global equation in F(z) using data from yearly semiannual amplitudes observed from 1997 through 2006. For incorporation into JB2008 the 81-day centered July average values are replaced by daily 81-day centered values of $\overline{F}_{10}$, $\overline{S}_{10}$, and $\overline{M}_{10}$. This is an approximation to the best fit equation. Using the daily 81-day centered values in Equations (4) and (5) result in an increase in the density error standard deviation of less than 1%.

Coef	Term	Value	STD
B_1	1	2.69E-01	1.84E-02
B_2	$\overline{F}_{SMJ}$	-1.18E-02	6.56E-04
B_3	$z\,\overline{F}_{SMJ}$	2.78E-02	1.92E-03
B_4	$z^2\overline{F}_{SMJ}$	-2.78E-02	1.20E-03
B_5	$z\,\overline{F}^2_{SMJ}$	3.47E-04	3.51E-05

Table 1. F(z) coefficient values with standard deviations (STD) from best fit results.

C. Semiannual G(t) Yearly Periodic Function

The yearly observed G(t) function, as previously discussed, consists of a Fourier series with 9 coefficients representing a quadannual variation. 28-day smoothed density difference data for each satellite was fitted with this Fourier series for each year. The density difference data is the accurate observed daily density values minus the Jacchia values without Jacchia's semiannual variation. The G(t) function was then obtained by normalizing to a value of 1.0 the difference between the minimum and maximum values for the year. The F(z) value for each satellite by year was used for the normalization. Figure 4 shows the results obtained for the year 1990 for the majority of the satellites. Note the tight consistency of the curves for all heights, covering over 800 km in altitude, which demonstrates the validity of using one G(t) function per year to represent the yearly semiannual phase for all altitudes. This tight consistency of the G(t) phase for all satellites also indicates that there is no significant latitude or local solar time effects with the semiannual density variation. This conclusion can be made because the majority of the satellites have moderate to high eccentricity orbits. This means that the great majority of the density sampling on each revolution occurs very close to the perigee location, and the daily density values computed from the orbit decays can be assigned to the argument of perigee latitude and local solar time, which is different for each satellite. The precession of the argument of perigee can be very slow (from zero to a few degrees per day), so if there is a latitude or local solar time semiannual effect the G(t) phase curves in Figure 4 should show significant differences because of the random nature of the argument of perigee locations. This is definitely not observed when comparing all of the individual satellite G(t) phase curves.

The next step in the study was to fit a yearly 9-term G(t) function for each year using the data for all the satellites for the year. Figure 4 also shows the yearly fit G(t) value for the year 1990. A small standard deviation was obtained for every year's fit, especially during solar maximum years. Figure 5 shows the yearly G(t) fits for 1999 through 2001, again showing the consistency of the semiannual phase at all altitudes for a given year. Also, it is readily apparent that the series changes dramatically from year to year. It was determined that during solar maximum the July minimum date can vary by as much as 80 days. During solar minimum the semiannual July minimum time variation is much smaller and appears to be flattened out in time.

As was done for the F(z) analysis it was decided to combine the new 81-day average indices in a linear function since each index is expressed in terms of F_{10} units and this approach worked very well for the F(z) analysis. A new solar index, representing long term EUV and FUV heating, was determined to be

$$\overline{F}_{SM} = 1.00\,\overline{F}_{10} - 0.75\,\overline{S}_{10} - 0.37\,\overline{M}_{10} \tag{6}$$

It was decided to start out using only annual and semiannual terms, instead of the JB2006 quadannual terms previously used, to try to represent the yearly semiannual phase variations. The yearly observed values had been fit with terms up to quadannual, but it was hoped that only terms up to semiannual needed to be included for a global model. The resulting equation was

$$\begin{aligned} G(t) &= C_1 + C_2\sin(\omega) + C_3\cos(\omega) + C_4\sin(2\omega) + C_5\cos(2\omega) \\ &+ \overline{F}_{SM}\left\{C_6 + C_7\sin(\omega) + C_8\cos(\omega) + C_9\sin(2\omega) + C_{10}\cos(2\omega)\right\} \end{aligned} \tag{7}$$

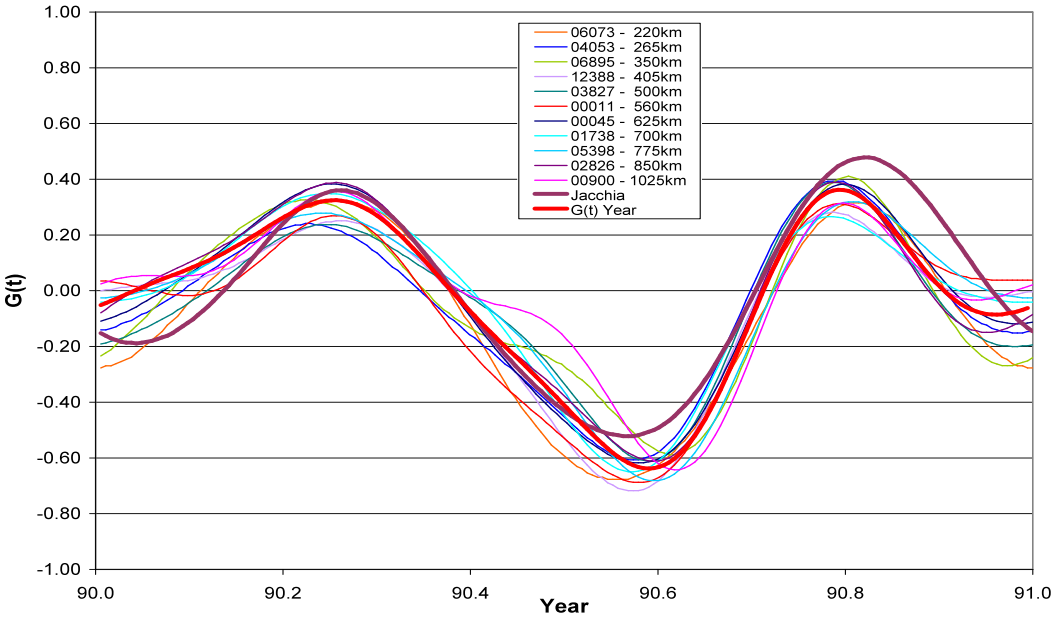

Figure 4. The individual satellite G(t) fits are plotted for 1990. The Jacchia model and yearly fit model are also shown.

The coefficients in Equation (6) are better defined than those for the F(z) index function specified by Equation (4). This is because density (G(t)) data and $\overline{F}_{SM}$ values were available throughout the entire year as opposed to using one July averaged value per year to derive Equation (4).

Table 2 lists the resulting C coefficient values with their standard deviations obtained from using Equation (6) for the solar index used in Equation (7). The standard deviations of the coefficients are all an order of magnitude smaller than the coefficient values except for the C_7 and C_8 $\overline{F}_{SM}$ annual terms, indicating a well determined set of coefficients.

Coef	Term	Value	STD
C_1	1	-3.63E-01	6.33E-03
C_2	$\sin(\omega)$	8.51E-02	9.23E-03
C_3	$\cos(\omega)$	2.40E-01	8.60E-03
C_4	$\sin(2\omega)$	-1.90E-01	8.61E-03
C_5	$\cos(2\omega)$	-2.55E-01	8.79E-03
C_6	$\overline{F}_{SM}$	-1.79E-02	3.63E-04
C_7	$\overline{F}_{SM}\sin(\omega)$	5.65E-04	5.39E-04
C_8	$\overline{F}_{SM}\cos(\omega)$	-6.41E-04	4.77E-04
C_9	$\overline{F}_{SM}\sin(2\omega)$	-3.42E-03	4.91E-04
C_{10}	$\overline{F}_{SM}\cos(2\omega)$	-1.25E-03	5.07E-04

Table 2. G(t) coefficient values with standard deviations (STD) from the best fit results.

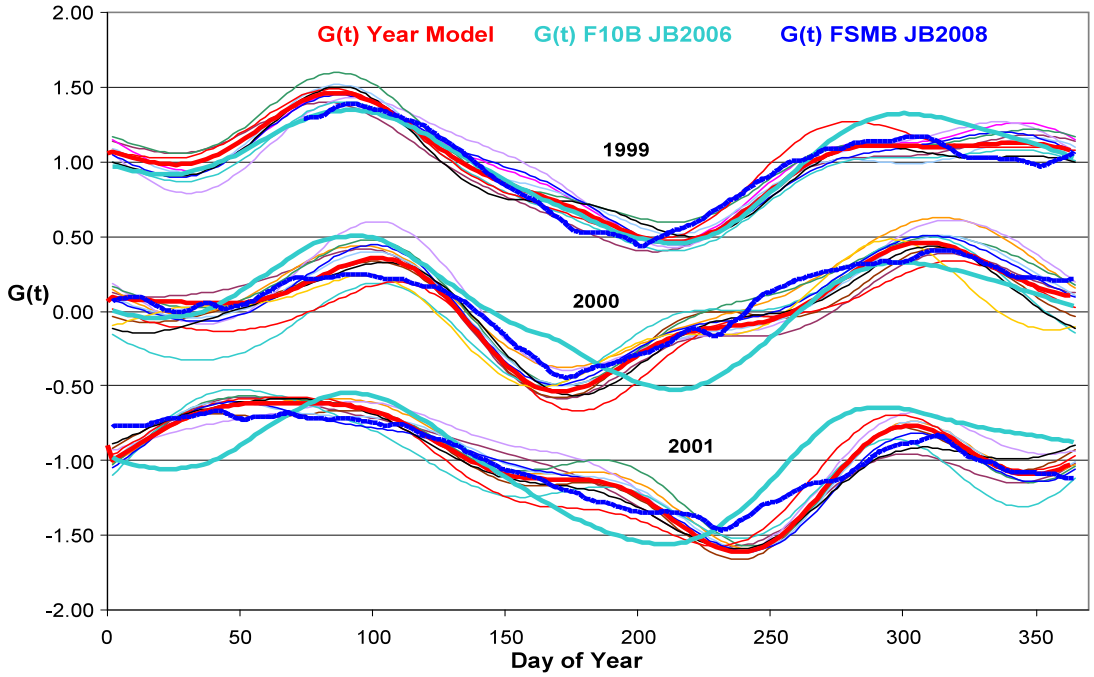

Figure 5. The individual satellite fits for 3 different years is shown. The Year G(t) Model is highlighted. Each set of curves for 1999 and 2001 has been offset by +1.00 and –1.00 respectively in G(t) for clarity. The JB2006 and new JB2008 model curves are also displayed.

The results of the new global model from Equations (6) and (7) are plotted in Figure 5 as the FSMB model. Also plotted are the yearly observed values for each year, and the original JB2006 $\overline{F}_{10}$ global model values. The 10-term new model results are impressive. Even with only annual and semiannual terms the new model accounts almost completely for the July minimum phase shifting which could not be captured in the $\overline{F}_{10}$ global model using even quadannual terms. This clearly demonstrates that the large majority of the variations observed in the semiannual density variation can be attributed to direct solar heating responses.

V. Geomagnetic Storm Modeling

A. Dst Index Description

The Disturbance Storm Time (Dst) index is primarily used to indicate the strength of the storm-time ring current in the inner magnetosphere. During the main phase of magnetic storms, the ring current becomes highly energized and produces a southward-directed magnetic field perturbation at low latitudes on the Earth's surface. This is opposite to the normal northward-directed main field. The index is determined from hourly measurements of the magnetic field made at four points around the Earth's equator and is available from World Data Center (A) at Kyoto[22].

Most magnetic storms begin with sharp rises in Dst, called the storm sudden commencement, in response to increased solar wind pressure. Following a southward turning of the interplanetary magnetic field, Dst decreases as ring current energy increases during the storm's main phase. During the recovery phase the ring current energy decreases and Dst increases until the storm's end. Traces of Dst show a transition from the early to late recovery phase characterized by significant changes in slope as the distribution of the ring current becomes symmetric in local-time. However, a significant fraction of magnetic storms manifest more complex structuring, with multiple main and partial recovery phases. Figure 6 for an example of the Dst events during a complex storm.

Use of Dst as a parameter of the energy deposited in the thermosphere during magnetic storms is more accurate than the use of the a_p index. The 3-hour a_p is an indicator of general magnetic activity over the Earth and responds primarily to currents flowing in the ionosphere and only secondarily to magnetospheric variations. The a_p index is determined by observatories at high latitudes which can be blind to energy input during large storms[23] and thus underestimate the effects of storms on the thermosphere.

As described below the thermosphere acts during storm periods as a driven-but-dissipative system whose dynamics is represented by a differential equation, with the changes in exospheric temperature change given as a function of Dst. To determine the exospheric temperature, and thereby the thermospheric density distribution at any time in a storm, it is necessary to integrate the differential equation for dTc starting at the storm commencement and proceeding throughout the entire storm period. Therefore, it is necessary to recognize where Dst measurements come in a particular storm's development.

An algorithm for determine the storm events was developed for locating in time the start, Dst minimum, recovery slope change, and final end of the storm. For practical reasons we define a magnetic disturbance as a storm only if the minimum Dst < -75 nT. We selected this value because disturbances with minimum Dst > -75 nT often lack identifiable storm profiles. Once the starting point of the storm is determined the algorithm steps forward in time until the minimum Dst value is obtained. This is defined as the end of the storm main phase. Because individual Dst traces may exhibit several local minima before reaching the deepest minimum, the algorithm specifies the real storm minimum point. Once the minimum is identified the algorithm continues stepping forward through the recovery phase until a major slope change is detected. From this point to the end of the storm the Dst slope is relatively shallow. It has been found that Dst takes much longer to recover than does the thermosphere[24]. To determine a "real" density recovery time more than 80 storms were analyzed. A linear fit of storm duration verse storm magnitude was obtained to give an equation for the approximate end time of the storm. The algorithm determines if the storm ends before this by examining when the Dst values are above the -75 nT limit. The lesser in time of the Dst limit or linear fit time is used for the end time. For complex storms (a second disturbance starts before the previous one ends) the algorithm determines the start, minimum, recovery slope change, and end point events of each storm. For a multiple storm the starting time of the second storm will be at the same time as the ending point of the first storm. Figure 6 shows the events for a complex storm. Even if the temperature and density are required at some point during the second storm it is important to start the temperature integration at the commencement of the first storm and carry it through into the second storm, since the thermosphere would already be heightened when the second disturbance began.

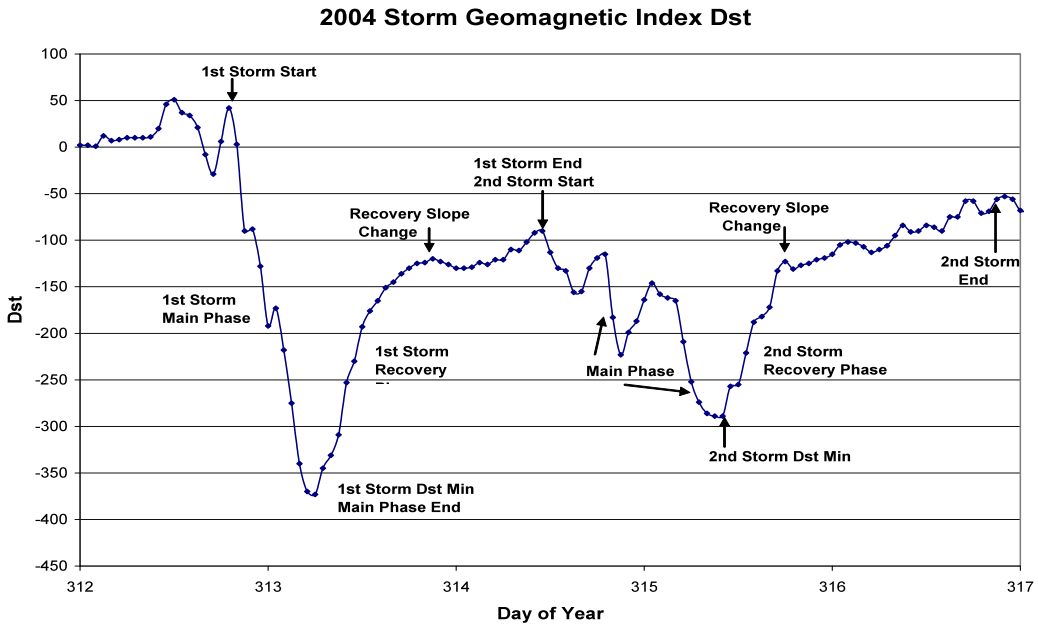

Figure 6. A multiple storm during 2004, showing the different storm events.

B. Dst Temperature Equations

Wilson et al.[25] suggested that on a global scale the storm-time thermosphere acts like a large thermodynamic system that never strays far from equilibrium. From an analysis of GRACE density measurements Burke et al.[24] further argued that the energy input to the thermosphere can be treated as a large driven-but-dissipative thermodynamic system, which can be described by differential equations similar to that of a resistor-inductor circuit. The driver is the magnetospheric electric field. They also demonstrated that Dst and storm-time changes of the exospheric temperature dTc share the same driver but have different relaxation time constants. By eliminating the electric field term from the two equations Burke et al.[24] established the following relation to determine exospheric temperature responses as a function of Dst.

$$dTc_1 = (1-\frac{1}{\tau_1})dTc_0 + S\left[Dst_1 - \left(1-\frac{1}{\tau_2}\right)Dst_0\right] \tag{8}$$

where τ_1 and τ_2 represent the temperature and Dst relaxation e-fold times. From an analysis of the GRACE data during 2004 storms Burke et al.[24] obtained values of $\tau_1 = 6.5$ hours and $\tau_2 = 7.7$ hours; the slope $S \approx 1.58$. Using these values in Equation (8) results in:

$$dTc_1 = 0.846\ dTc_0 + 1.58\left[Dst_1 - 0.870\ Dst_0\right] \tag{9}$$

The subscript 1 above represents the value at one time step beyond the subscript 0 point. The storm event algorithm described above was used to determine the event times for the storm being considered. Equation (9) was then integrated from storm commencement time until storm end time, producing exospheric temperature change values every hour throughout the storm period. These temperature change values were input into the JB2008 model to represent the geomagnetic storm effects at all points throughout the storm.

Comparisons of orbit averaged density values were obtained using results from Equation (9) and the CHAMP and GRACE accelerometer densities. Since it had been shown that the Dst index was proportional to "global" thermospheric variations it was decided to use orbit averaged values for all the comparisons. Using Equation (9) produced good correlations of the JB2008 model density with the accelerometer data, but it was noticed that the model and data deviations became greater as the maximum storm magnitude decreased among all storms. It was decided to re-determine the value of the slope S while accepting Burke's values of both the relaxation parameters. An optimization study during the JB2008 development determined that these τ_1 and τ_2 values were the best to use. This was done for a number of storms varying from minor to major. The slope value for each storm was optimized by minimizing the differences of the JB2008 model orbit averaged density ratios using Equation (9) with the orbit averaged accelerometer ratios during the main phase region. The newly determined slope for each storm was then plotted as a function of the storm Dst minimum value, and also plotted as a function of the ΔDst (minimum-maximum) value. The Dst minimum values produced the least scatter of the data. Figure 7 is a plot of the main phase slope with respect to the Dst minimum value.

Equation (10) represents the new quadratic function for S as a function of the Dst minimum (Dst_{MIN}) value. If $Dst_{MIN} < -450$ then $S = -1.40$.

$$S = -1.5050\,x\,10^{-05}\,(Dst_{MIN})^2 - 1.0604\,x\,10^{-02}\,Dst_{MIN} - 3.20 \tag{10}$$

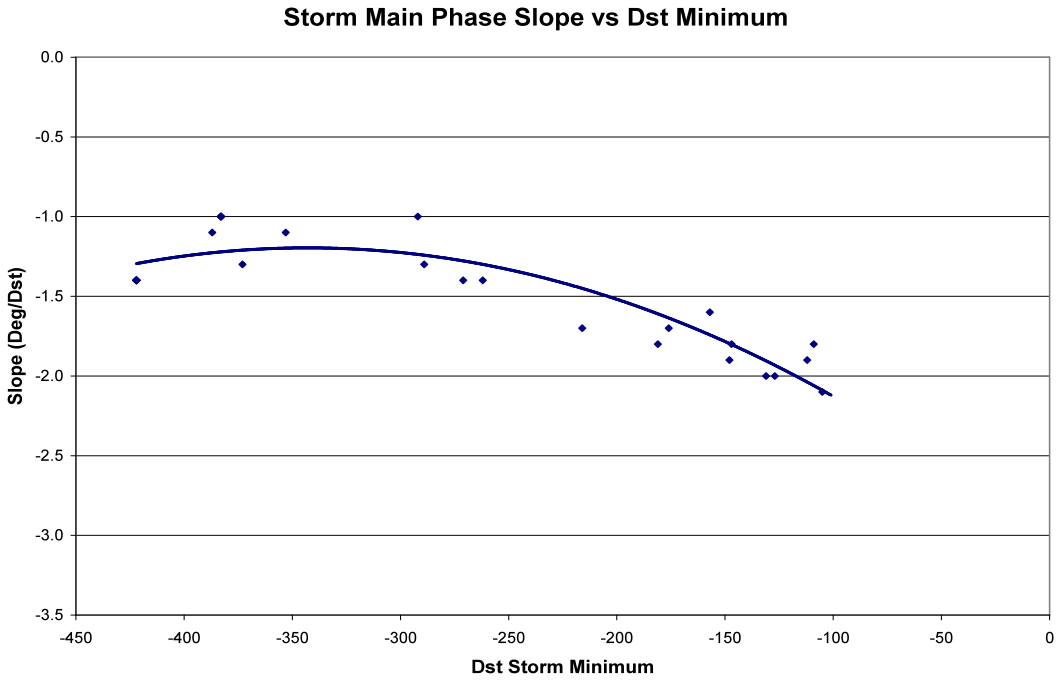

Figure 7. Optimized storm main phase slope S values as a function of storm Dst minimum.

Using this new slope quadratic equation produced very consistent results for storms of all magnitudes. However, a few additional adjustments had to be made to produce even better results. It was discovered that starting the dTc integration at dTc = 0 for the storm commencement time sometimes resulted in large negative temperature changes at storm start. This was due to the fact that the thermosphere was already at a slightly heightened temperature state. Therefore, it was decided to start the dTc integration with a value equal to a temperature change obtained from Jacchia's 1970 geomagnetic storm equation using the 3-hour a_p value (with a 6.7 hour lag time) at the start time. Further analysis of all the storms showed that this produced better results than using an initial zero value. A second adjustment during this main phase analysis occurred during sub-storms when the Dst variations became positive. The density values did not drop as expected. In fact the accelerometer and HASDM density changes during these time periods continued to increase even though the Dst value was increasing during these short main phase time periods. Additional equations were developed for these time periods:

$$dTc_1 = dTc_0 - S_{FAC}\, S(Dst_1 - Dst_0) \tag{11}$$

where the best factor S_{FAC} was found to be 0.3 for all storms. The S value was obtained from Equation (10). Since S is negative and ΔDst is positive during these time periods Equation (11) has the effect of continuing to increase the temperature change (and therefore the density) even though Dst is increasing during these times. Using Equation (11) in the JB2008 model produced better correlations with the accelerometer data. Finally, it was noticed that a small lag time was needed to better represent the main phase density increase, especially during small storm events. It was determined that for large storms (Dst < -350), moderate storms (-350 < Dst < -250), and minor storms (-250 < Dst) lag times of 0, 1, and 2 hours respectively better represented the main phase density changes.

The recovery phase was addressed after the main phase equations had been developed. Equation (9) and (10) were initially used to represent the recovery phase changes. This did work well except for a few outstanding cases. Each storm was re-optimized for the recovery phase by optimizing the slope for this phase only. However, the recovery phase of the large 2003 multiple storm did not fit the accelerometer density data even with optimizing Equation (9) just for the recovery phase. It was decided to optimize τ_1 and τ_2 for this phase. After many trials the best fit for the 2003 multiple storm was $\tau_1 = \infty$ and $\tau_2 = 1$. A new slope was then obtained for this storm, and the resulting equation for this large storm was:

$$dTc_1 = 1.00\, dTc_0 + 0.13\, Dst_1 \quad (12)$$

The next step was to determine the varying slopes for storms of other magnitudes. Surprisingly Equation (12) was found to be the best representation for all the other storms representing all magnitudes. This single slope value was excellent for the entire recovery phase up to the recovery slope change.

The final equation fitting was for the period covering the recovery slope change to the end of the storm. It was decided to use the simpler Equation (13) below since it was supposed that for this time period the ring current had disconnected from the ionosphere, which meant that the function representing the ring current energy release was unknown.

$$dTc_1 = dTc_0 + S(Dst_1 - Dst_0) \quad (13)$$

The resulting slope S was found to be a constant -2.5 to best fit all the storms. It was found sometimes that dTc became negative towards the "end" time of the storm because the end time was not defined correctly. To make sure this didn't occur the algorithm sets dTc = 0 when the integration step produces a negative dTc. Finally, for Dst "non-storm" periods (Dst>-75) JB2008 uses Jacchia's 1970 dTc equation as a function of the 3-hour a_p value. When the JB2008 storm computation algorithm has determined that no Dst storm is present, then if $a_p > 50$, a value of 50 is used for the dTc. This avoids large spurious density increases due to high a_p values when no storm really exists.

C. Dst Modeling Results

Using these equations for each of the 3 different storm phases results in very good comparisons of the JB2008 density values with the accelerometer and HASDM values. Figures 8 and 9 below are examples of plots of model density ratios during two major storm periods. Yearly average density values were obtained for the CHAMP and GRACE data. The displayed CHAMP density ratios are orbit averaged values / yearly average, and then multiplied by 1.17 to adjust to the HASDM values. The 17% factor is based on averaging the CHAMP/HASDM ratios over the 2001-2005 time period. A factor of 0.74 was obtained for the GRACE/HASDM ratios based on all data from 2002 through 2005. The HASDM values plus other model values are orbit averaged (along the CHAMP or GRACE orbit), with all ratios based on each year's CHAMP (or GRACE) average density value. Figure 8 shows the 2004 major storm period when the GRACE accelerometer data was available, and Figure 9 shows the 2003 major storm period when the CHAMP accelerometer data was available. The HASDM ratios agree extremely well with the accelerometer data following the single calibration for each data set. The JB2008 model also is very consistent with the density changes throughout each storm, indicating that the JB2008 model temperature equations are working extremely well for these orbit altitudes of 400 to 500 km. The MSIS (NRLMSIS) density values are mostly low at storm peak times during the largest storms, which is consistent with the results previously reported by Burke et al[24]. The Jacchia 70 (J70) values are extremely high at peak storm times because they are based on single a_p values which are maxed out at a value of 400 when the magnetometers are saturated. For the 2003 storms in Figure 9 both the MSIS and J70 values before and after the storm periods are much too high, a result of not correctly modeling the solar EUV during this period when the 27-day F_{10} values were exceptionally high.

Finally, Figure 10 shows 1-standard deviation model density errors as a function of storm magnitude. The values were obtained as percent density differences from the calibrated orbit averaged accelerometer data, from both CHAMP and GRACE, and the different model orbit averaged values. The results show that the JB2008 model is a major improvement over modeling density changes during large geomagnetic storms. The HASDM modeling is the best at under a 10% sigma, which is expected since it accounts for real time density changes. The J70 modeling is the worst since it is based on computing a density from a single 3-hour a_p value, while the MSIS model uses a history of a_p values for 57 hours prior to the time of interest.

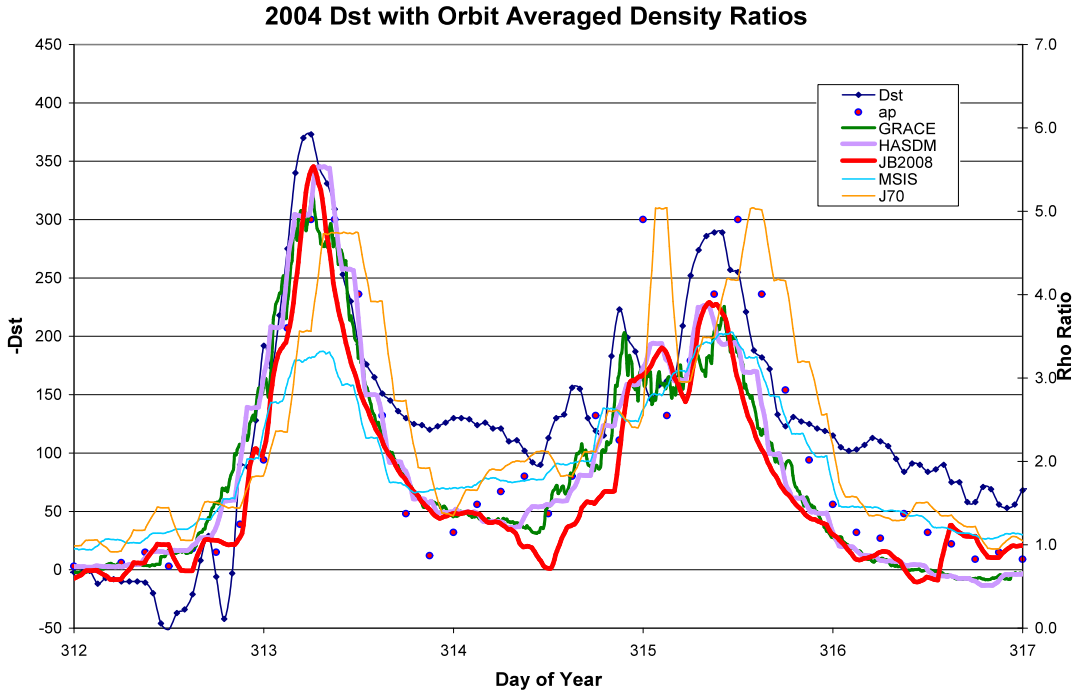

Figure 8. Major 2004 storms with Dst, a_p (left scale) , and density (Rho) ratios displayed. The density ratios are based on orbit averaged model density values / GRACE 2004 density average. See text for additional information.

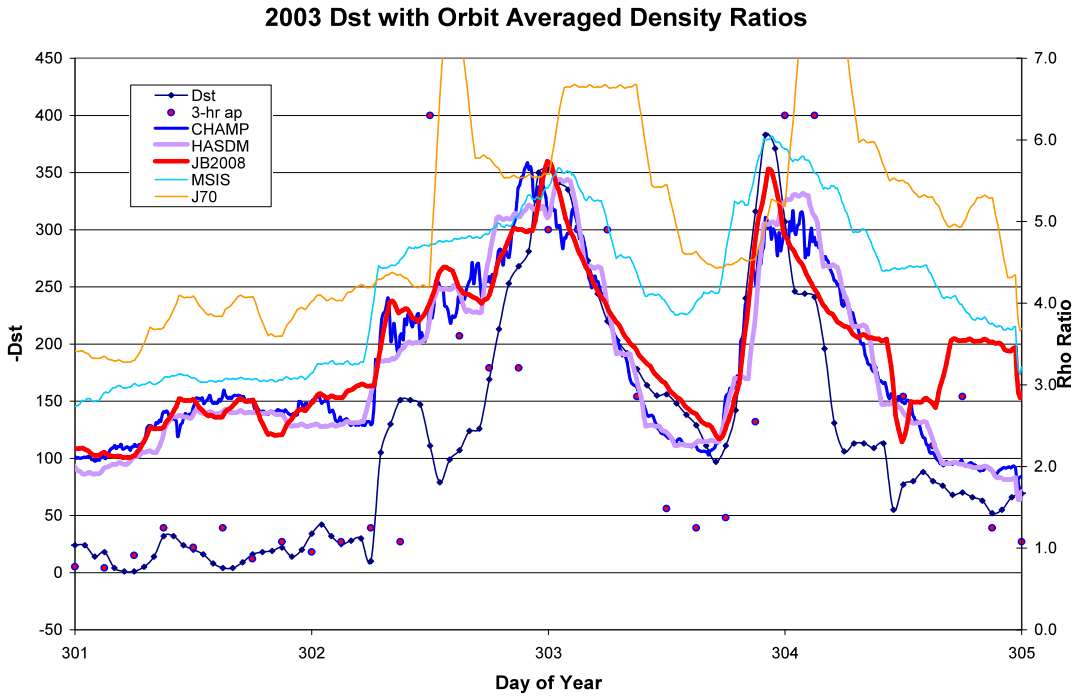

Figure 9. Major 2003 storms with Dst, a_p (left scale), and density (Rho) ratios displayed. The density ratios are based on orbit averaged model density values / CHAMP 2003 density average. See text for additional information.

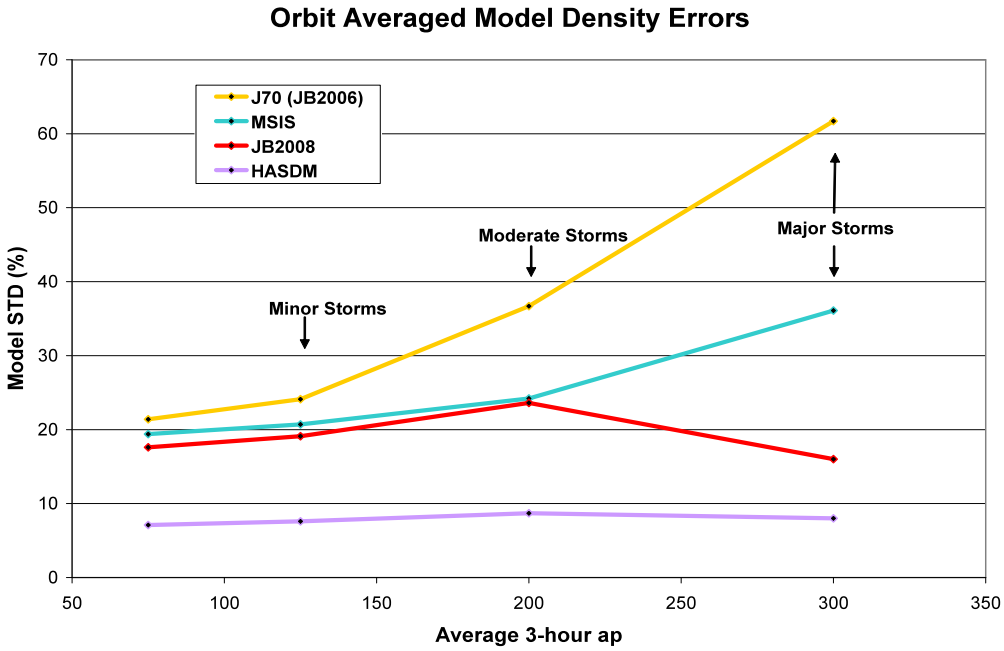

Figure 10. Model density 1-standard deviation errors as a function of a_p ranges representing storm magnitudes. Values are based on orbit averaged percent density differences between the calibrated accelerometer data, from both CHAMP and GRACE, and the different model values. JB2006 uses the same geomagnetic storm modeling as J70.

VII. JB2008 Model Usage

A detailed description of the model, Fortran source code, indices, and published papers can be obtained at the web site http://sol.spacenvironment.net/~jb2008/. On the main web page are selections for an introduction to the model, all the papers published with regard to the JB2006 and JB2008 development, a separate solar and geomagnetic index page, the Fortran source code for the JB2008 model and driver program, plus selections for author contacts, figures, and the SET web site. On the indices page is listed a selection for the Fortran source code use in developing the new temperature index from the Dst values, the new temperature index, and the Dst and ap indices. A short description of the Fortran programs follows.

The Fortran source code for the JB2008 model consists of two source code files. One file is for the JB2008 model subroutine, including all associated subroutines called by the model. The inputs and outputs, along with the publication equation references, are listed within the code. The second Fortran source file is a test driver program, JB2008DRV, with associated subroutines required to call the JB2008 model program. Also included are a solar index file, the geomagnetic storm temperature index file, and satellite geographic position test input and output files. In this driver program the solar indices are obtained from the SOLFSMY subroutine that uses different lag times for retrieving the different solar indices. A test input file of satellite positions is used to compute the position parameters required for input to the JB2008 model. Please note that the satellite longitude is converted to a right ascension value required by JB2008. A subroutine for computing the sun's position is also included. The geomagnetic storm index used by JB2008 is the exospheric temperature change. This index is described in the following paragraph. For every input test satellite position the JB2008 model is called to compute the density value, and a test output file is written with the density and indices used in the generation of the density value. This output should be compared with the sample output provided with the code to insure the program is running correctly.

The geomagnetic storm temperature index used by JB2008 reflects the change in the exospheric temperature. This temperature change is computed from the change in the Dst index during a storm. Outside of storm periods this index is computed from Jacchia's 1970 equation using the 3-hour ap value. Since the temperature change is global in nature it only needs to be computed once independent of any geography (latitude, longitude, altitude) when new Dst values are obtained. The web site will provide the

continuously updated temperature index on a daily basis as new Dst values are obtained and added to the Dst file. The temperature index file is then used as an input to the JB2008 model. Refer to the test driver JB2008DRV source code for its usage. Fortran source code used to compute this temperature change is included in the DTCMAKEDR file. The file has a driver program that inputs Dst values, determines geomagnetic storm event times, and integrates the temperature equations as a function of the Dst changes throughout an entire storm period. Refer to the discussion in the JB2008 model publication paper. This computer program is provided for reference only since the temperature index file will be generated on a daily basis and provided at the web site. To run this program requires the Dst file and the 3-hour ap file, both of which are also found on the web site.

VIII. Conclusions

The following results have been obtained using the new JB2008 model:

1. Use of new global exospheric temperature equations based on EUV and FUV solar indices significantly improves density modeling, especially at solar minimum times.
2. Density standard deviation errors during non-storm periods have been reduced by over 5% from previous Jacchia 70 and NRLMSIS models.
3. Use of new semiannual density variation equations using multiple 81-day averaged solar indices now accounts for major yearly semiannual density changes due to changing long term EUV heating.
4. Use of the Dst index as a replacement for a_p greatly reduces density errors, especially during major geomagnetic storm periods. This error reduction is from over 60% for Jacchia 70 and over 35% for NRLMSIS, to 16% for JB2008 during major storms.

Significant improvements in empirical density modeling have been obtained using the new JB2008 model incorporating new solar indices, a new semiannual variation equation, and a new geomagnetic index. The new model, Jacchia-Bowman 2008 (JB2008) provides standard deviations of approximately 9-10% at 400 km, a significant decrease from 16% previously obtained using the Jacchia 70 model.

Acknowledgments

We would like to thank Sean Bruinsma, CNES, for providing CHAMP accelerometer densities, and Byron Tapley and Minkang Chen, University of Texas, for providing GRACE accelerometer densities.

References

1. Bowman, B.R., W. K. Tobiska, F.A. Marcos, C. Valladares, “The JB2006 empirical thermospheric density model,” *Journal of Atmospheric and Solar-Terrestrial Physics,* 2007, doi:10.1016/j.jastp.2007.10.002.
2. Marcos, F.A., "Accuracy of atmospheric drag models at low satellite altitudes," *Advances in Space Research*, 10, 417, 1990.
3. Bowman, B.R., “The semiannual thermospheric density variation from 1970 to 2002 between 200-1100km,” AAS 2004-174, *AAS/AIAA Spaceflight Mechanics Meeting*, Maui, HI, February, 2004.
4. Bowman, B.R., W. K. Tobiska, M.J. Kendra, “The thermosphere semiannual density response to solar EUV heating,” *Journal of Atmospheric and Solar-Terrestrial Physics,* 2008, doi:10.1016/j.jastp.2008.04.020.
5. Bowman, B.R., et al., “A method for computing accurate daily atmospheric density values from satellite drag data,” AAS 2004-179, *AAS/AIAA Spaceflight Mechanics Meeting*, Maui, HI, Feb, 2004.
6. Jacchia, L.G., “New static models of the thermosphere and exosphere with empirical temperature profiles,” *Smithson. Astrophys. Special Report 313*, 1970.
7. Jacchia, L.G., “Revised static models of the thermosphere and exosphere with empirical temperature profiles,” *Smithson. Astrophys. Special Report 332*, 1971.

8. Bowman, B.R., "True satellite ballistic coefficient determination for HASDM," AIAA-2002-4887, *AIAA/AAS Astrodynamics Specialist Conference*, Monterey, California, August, 2002.
9. Storz, M.F., et al., "High accuracy satellite drag model (HASDM)," AIAA 2002-4886, *AIAA/AAS Astrodynamics Specialist Conference*, Monterey, Ca, August, 2002.
10. Bowman, B. R., M.F. Storz, "High Accuracy Satellite Drag Model (HASDM) Review," AAS 2003-625, AAS/AIAA Astrodynamics Specialist Conf., Big Sky, Mt, August, 2003.
11. GFZ, Potsdam, www.gfz-potsdam.de/pb1/op/champ
12. Bruinsma, S., D. Tamagnan, R. Biancale, "Atmospheric densities derived from CHAMP/STAR accelerometer observations," *Planet. Space Sci*, 52, 297-312, 2004.
13. Tapley, B.D., S. Bettadpur, M. Watkins, C. Reigber, "The gravity recovery and climate experiment: Mission overview and early results," *Geophys. Res. Lett.*, 31,L09607, 2004, doi:10.1029/2004GL019920.
14. University of Texas, www.csr.utexas.edu/grace
15. Bowman, B.R., et al., "Improvements in modeling thermospheric densities using new EUV and FUV solar indices," AAS 2006-237, *AAS/AIAA Spaceflight Mechanics Meeting*, Tampa, Fl, January, 2006.
16. Marcos, F. A., J. O. Wise, M. J. Kendra, N. J. Grossbard, B.R. Bowman, "Detection of a long-term decrease in thermospheric neutral density", *Geophy. Res. Lett.*, 32, 2005, doi.10.1029/2004GL021269.
17. Marcos, F.A., et al., "Accuracy of Earth's thermospheric neutral density models," AIAA 2006-6167, *AIAA/AAS Astrodynamics Specialist Conference*, Keystone, CO, August, 2006.
18. Picone, J.M., A.E. Hedin, D.P. Drob, A.C. Aikin, "NRLMSISE-00 empirical model of the atmosphere: statistical comparisons and scientific issues," *J. Geophys. Res.* 107 (A12),1468, 2002.
19. Paetzold, H.K., H. Zschorner, "The structure of the upper atmosphere and its variations after satellite observations," Space Research II, 958, North-Holland Publ. Co., Amsterdam, 1961.
20. King-Hele, D.G., J. Hingston, "Air density at heights near 190km in 1966-7 from the orbit of Secor 6," *Planet. Space Sci.*, 16, 675, 1968.
21. Roble, R.G., "Solar cycle variation of the global mean structure of the thermosphere," Proceedings of a workshop, The National Center for Atmospheric Research, Nov. 9-11, 1987.
22. Kyoto web site: (http://swdcwww.kugi.kyoto-u.ac.jp/wdc/Sec3.html).
23. Huang, C. Y., W. J. Burke, "Transient sheets of field-aligned current observed by DMSP during the main phase of a magnetic superstorm," *J. Geophys. Res.,* 109, A6303, 2004, doi: 10.1029/2004JA010583,
24. Burke, W.J., et al., "The stormtime global thermosphere: A driven-dissipative thermodynamic system," journal review in progess.
25. Wilson, G.R., et al., "Response of the thermosphere to Joule heating," *J. Geophys. Res.*, 111, A10314, doi: 10.1029/2006-JA011274.
26. Tobiska, W. K., S.D. Bouwer, and B.R. Bowman, "The development of new solar indices for use in thermospheric density modeling," J. Atm. Solar Terr. Phys., 70, 803-918, 2008.
27. Tobiska, W.K., "Systems-Level Space Environment Specification for Satellite and Ground System Operations," AIAA Aerospace Sciences Meeting, AIAA-2005-0069, January 2005.
28. ISO 21348:2007, Space Environment (natural and artificial) – Process for determining solar irradiances, International Standards Organization (ISO), Geneva, 2007.